ChemComm

COMMUNICATION

View Article Online
View Journal | View Issue

Cite this: *Chem. Commun.*, 2017, 53, 10512

Received 1st July 2017,
Accepted 29th August 2017

DOI: 10.1039/c7cc05098d

rsc.li/chemcomm

Calculation and experimental measurement of paramagnetic NMR parameters of phenolic oximate Cu(II) complexes†

Daniel M. Dawson, Zhipeng Ke, Frederick M. Mack, Rachel A. Doyle, Giulia P. M. Bignami, Iain A. Smellie, Michael Bühl* and Sharon E. Ashbrook *

We present a strategy for predicting the unusual ^{1}H and ^{13}C shifts in NMR spectra of paramagnetic bisoximato copper(II) complexes using DFT. We demonstrate good agreement with experimental measurements, although ^{1}H–^{13}C correlation spectra show that a combined experimental and theoretical approach remains necessary for full assignment.

In recent years, paramagnetic NMR (or "pNMR") has developed greatly, with systems from metalloproteins[1] (dilute, isolated spins) to metal–organic frameworks[2–4] (denser networks of potentially coupled spins) and metal oxides[5] (very dense networks of highly coupled spins) being studied. For dilute spins, the NMR conditions can be selected such that the signal from nuclei near the paramagnetic centre is "invisible" owing to rapid relaxation and only the longer-range through-space pseudocontact shifts are observed.[1] These are generally on the order of a few ppm and occur over distances such that the unpaired electron can be treated as a point spin, resulting in a simple $1/r^3$ relationship with the shift. For dense spin networks such as transition metal oxides, it may be possible to assign the NMR spectra by analysis of bonding pathways (*via* oxygen).[5] However, in the intermediate regime, including materials such as catalytically-active transition metal complexes and metal–organic frameworks (MOFs), both the through-bond Fermi contact and through-space pseudocontact interactions affect the observed NMR spectrum and assignment can be both nontrivial and counterintuitive.[2,6–9] For example, in the ^{13}C NMR spectrum of the MOF HKUST-1 (Cu_3btc_2, btc = benzene-1,3,5-tricarboxylate),[10] the broadest resonance, shifted most by paramagnetic interactions, is not the carboxylate C (separated from Cu^{2+} by just two bonds), but rather the adjacent quaternary C (three bonds from Cu). This assignment was confirmed using the relatively costly and time-consuming approach of specific ^{13}C labelling in conjunction with ^{1}H–^{13}C cross polarisation (CP) NMR, which is generally inefficient for paramagnetic materials.[2] It would, therefore, be desirable to have a more general assignment method that does not rely on the development of bespoke synthetic pathways for efficient isotopic enrichment. Owing to the rapid MAS rates (necessitating the use of small rotors with, consequently, small sample volumes) required for high-resolution pNMR spectra, sensitivity is inherently low and it would, therefore, also be advantageous to be able to predict shifts prior to the experimental measurement, particularly as resonances can be several hundred ppm away from their typical diamagnetic range.

Periodic density functional theory (DFT) calculations have enjoyed great success in solid-state NMR, allowing the optimisation of experimental structures to an energy minimum and the subsequent calculation of highly accurate NMR parameters.[11–13] However, pNMR DFT calculations are still in their relative infancy, particularly for periodic solids. The field is more advanced for molecular calculations, which have successfully been used to assign the NMR spectra of a range of complexes of interest.[14–17] Recently, we reported the calculated and experimental NMR parameters for **1** (see Fig. 1).[6] This material provides a typical example of the non-intuitive nature of the paramagnetic shifts: at 298 K the ^{13}C resonance with the highest shift (1006 ppm) corresponds to C3, which is bonded to the H with the lowest shift (−5.4 ppm) and the ^{13}C resonance with the second-highest shift (963 ppm) corresponds to C7, which is bonded to the H with the highest shift (272 ppm). The calculated shifts for the complex (and their variation with temperature) were in good agreement with experiment, particularly given that the calculations were carried out for a single gas-phase molecule rather than the periodic solid. Exploratory calculations suggested a negligible ($J \approx 0.3$ cm^{-1}) coupling between spins on adjacent molecules and this, along with other long-range packing effects, led to only small shift differences of up to 4.7 ppm for the most shifted ^{1}H and 56.9 ppm (~5% of the total shift range) for the most shifted ^{13}C. By combining the predicted peak positions with their calculated temperature dependence (assumed to be linear with $1/T$, where a plot of δ_{iso} *vs.* $1/T$ yields a gradient $d\delta_{iso}/d(1/T)$ and a y intercept δ_{iso}^{∞}),

School of Chemistry, EaStCHEM and Centre of Magnetic Resonance, University of St Andrews, North Haugh, St Andrews, Fife, KY16 9ST, UK. E-mail: sema@st-andrews.ac.uk, mb105@st-andrews.ac.uk

† Electronic supplementary information (ESI) available: Experimental and computational details, additional calculated and experimental pNMR parameters. See DOI: 10.1039/c7cc05098d

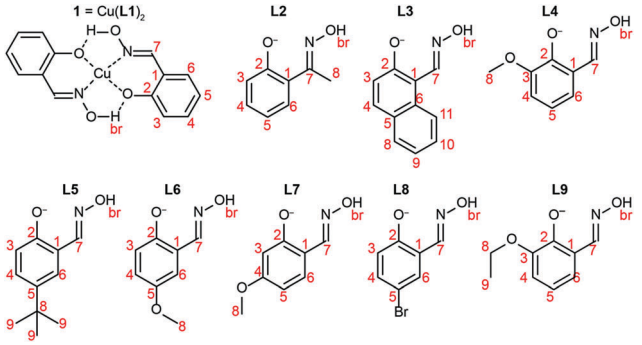

Fig. 1 The structures of bis(salycylaldoximato)copper(II) (**1** = Cu(**L1**)$_2$) and the functionalised ligands considered, where compound **N** has the formula Cu(**LN**)$_2$. The numbering schemes used are indicated in red.

all resonances could be assigned. As discussed above, the attraction of using DFT calculations to assign the NMR spectra of paramagnetic materials is that they can be carried out in advance of the experiment and can, thus, be used to guide spectral acquisition as well as assignment. Here we extend this investigation to **2–9** (see Fig. 1), comparing DFT predictions with multidimensional multinuclear NMR spectra. To be able to distinguish between positional isomers (*cf.* **4**, **6**, **7**) or to account for subtle changes such as replacing a H atom with a Me group (*cf.* **1**/**2** or **4**/**9**) would greatly improve the predictive power of the calculations and increase the potential of the joint experimental/theoretical approach as a structural tool.

As described in the ESI,† we employed our recently introduced computational methodology[6] to optimise molecular complexes in the gas phase and calculate their pNMR parameters. Fig. 2a shows the highest occupied molecular orbital (HOMO) for the representative example of **6**, which can be seen to arise from an interaction between the $d_{(x^2-y^2)}$ orbital of Cu and a σ-antibonding orbital of the ligands. As shown by the spin density isosurface of **6** (Fig. 2b), the presence of the unpaired electron within the σ framework of the ligands leads to large spin density on atoms within 4 bonds of Cu, but almost negligible spin density on the periphery of the molecule. The partial s character of the HOMO on atoms close to the Cu (see ESI†) leads to large computed hyperfine couplings for these nuclei, and Fig. 2c and d show the predicted ^{1}H and ^{13}C peak positions for **2–9** at 298 K. While the calculations indicate only minor substituent effects on the ^{1}H shifts, larger effects are predicted for ^{13}C, where some resonances in the aromatic region can re-order.

Fig. 3a shows the ^{1}H MAS NMR spectrum of **6**, which contains the expected six resonances between 268 and −5.2 ppm. The spectrum was recorded in five steps (see ESI† for details). Fig. 3b shows the ^{13}C MAS NMR spectrum of **6** and, again, the expected 8 resonances are observed, between 1020 and 54 ppm. The spectrum was recorded in four steps (see ESI† for details). As can be seen in Fig. 3c and d, the positions of many of the resonances in both spectra vary significantly with temperature, confirming large through-bond interactions with the unpaired electron. The range of observed shifts and their temperature dependence are in good agreement with the picture obtained from DFT calculations.

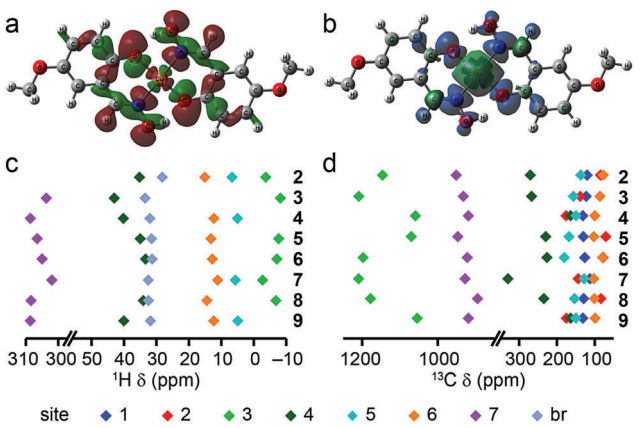

Fig. 2 (a) α-HOMO and (b) spin density isosurfaces of **6**, plotted at 0.02 and 0.0004 a.u., respectively. Calculated positions of (c) ^{1}H and (d) ^{13}C resonances (at 298 K and neglecting the substituents) for **2–9**.

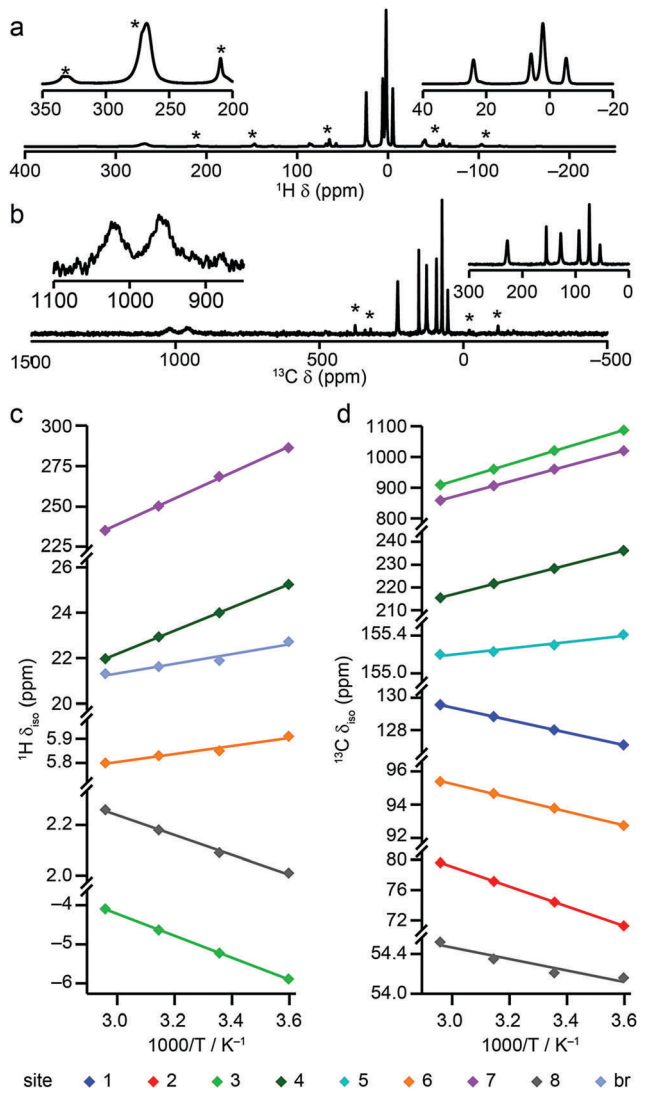

Fig. 3 (a) ^{1}H and (b) ^{13}C (14.1 T, 298 K, 37.5 kHz MAS) NMR spectra of **6**. Variation in (c) ^{1}H and (d) ^{13}C peak positions of **6** as a function of 1/*T*. * denotes a spinning sideband.

Partial spectral assignment was achieved using ^{1}H–^{13}C heteronuclear correlation (HETCOR) experiments. Ideally, these would select for magnetisation transfer through the scalar coupling with a mixing time selective for $^{1}J_{CH}$. However, this would be several ms, during which much of the magnetisation would return to thermal equilibrium (T_1 relaxation constants for C1–7 (not reported) were typically $<$200 ms). Therefore, magnetisation was transferred *via* the through-space dipolar coupling using cross polarisation (CP) with a spin-lock duration of 100 μs to ensure transfer over distances similar to a C–H bond. The spectrum of **6** (shown in Fig. 4) was recorded with frequency stepping for both ^{1}H and ^{13}C (see ESI† for details). The HETCOR spectrum allows identification of the expected five CH pairs and three quaternary C species. The ^{1}H resonance at 21.9 ppm that does not correlate to ^{13}C corresponds to Hbr.

Having identified the CH and C species from the HETCOR spectra, assignment of all observed resonances was carried out by comparison with the DFT calculations, with Table 1 giving the final assignments for **6** (see ESI† for all experimental and computed data and final assignments for **2–5** and **7–9**). In several cases (for example, C1 and C6 in **4** – see ESI†), assignment based only on the calculated position of the resonances is incorrect, but the sign and magnitude of $d\delta_{iso}/d(1/T)$ and the "diamagnetic" shift contribution, δ_{iso}^{∞}, combined with the connectivity from the HETCOR spectrum, allows a complete assignment to be made. It is clear from such cases that measurement of the temperature dependence of δ_{iso} is vital to enable complete assignment, and the $d\delta_{iso}/d(1/T)$ and δ_{iso}^{∞} values presented here allow comparison of experimental and computed spectra at any given temperature (in the limit of the high-temperature regime model implicit in the calculations). It is also noticeable that C1 and C2 have much smaller paramagnetic shifts and narrower lines than C3 and C7, despite similar proximity to the Cu centre. Although somewhat surprising, this can be explained by the spin density plot in Fig. 2b, which shows the interaction is highly directional, and emphasises the need to combine accurate DFT calculations with experiment to correctly assign all resonances.

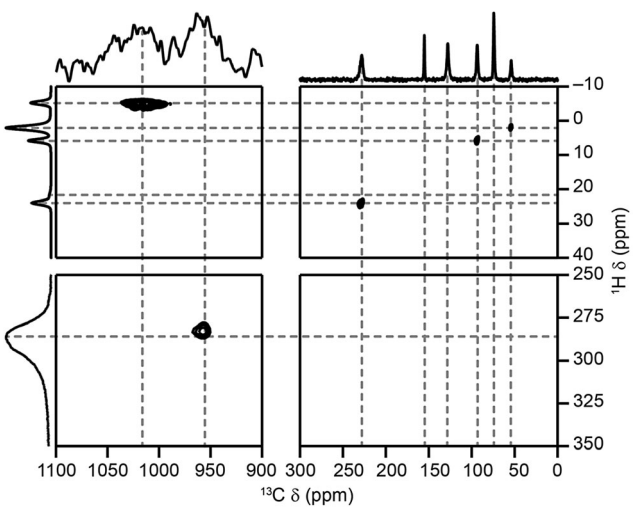

Fig. 4 (14.1 T, 37.5 kHz MAS, 298 K) ^{1}H–^{13}C CP HETCOR spectrum of **6** recorded with a contact time of 100 μs. Each region was recorded separately with different acquisition conditions (see ESI†) and contour levels are arbitrary.

Table 1 Calculated (DFT) and experimental (exp.) pNMR parameters for **6**

	δ_{iso} at 298 K (ppm)		$d\delta_{iso}/d(1/T)/10^{-6}$ K		δ_{iso}^{∞} (ppm)	
	Exp.	DFT	Exp.	DFT	Exp.	DFT
H3	−5.2	−7.1	$-2.80(3) \times 10^{3}$	-4.19×10^{3}	4.18(9)	6.93
H4	24.0	33.4	$5.11(2) \times 10^{3}$	7.80×10^{3}	6.85(7)	7.19
H6	5.9	12.8	$1.6(2) \times 10^{2}$	1.90×10^{3}	5.31(7)	6.39
H7	268	305	$8.0(2) \times 10^{4}$	8.85×10^{4}	−2(6)	8.11
H8	2.1	3.3	$-3.9(2) \times 10^{2}$	−77.3	3.42(5)	3.53
Hbr	21.9	31.3	$2.1(4) \times 10^{3}$	6.18×10^{3}	15(1)	10.59
C1	128	126.2	$-3.916(6) \times 10^{3}$	2.51×10^{3}	141.16(2)	117.8
C2	74	77.7	$-1.303(3) \times 10^{4}$	-2.55×10^{4}	118.14(9)	163.1
C3	1020	1198	$2.79(2) \times 10^{5}$	3.19×10^{5}	82(5)	128.0
C4	228	226.3	$3.24(3) \times 10^{4}$	2.84×10^{4}	119.8(9)	130.9
C5	155	180.5	$3.3(5) \times 10^{2}$	7.60×10^{3}	154.2(1)	155.0
C6	94	79.0	$-4.17(7) \times 10^{3}$	-1.07×10^{4}	107.7(2)	114.8
C7	960	922	$2.53(2) \times 10^{5}$	2.28×10^{5}	111(5)	158.3
C8	54	55.3	$-5.8(12) \times 10^{2}$	2.17×10^{2}	56.2(4)	54.6

Fig. 5a presents a plot of the calculated ^{13}C δ_{iso} at 298 K against the experimental values for the compounds in Fig. 1. It can be seen that excellent agreement is observed for the resonances with large paramagnetic shifts (C3, C4 and C7), but that, where the shift is closer to the diamagnetic region (either because the C is many bonds from Cu (as in C5) or because of cancellation of positive and negative spin density, as in C1 and C2), the error is greater. Fig. 5b shows a plot of calculated ^{13}C $d\delta_{iso}/d(1/T)$ (which is proportional to the hyperfine coupling constant) against the experimental values for the same compounds. Again, generally excellent agreement is achieved, although it can be seen from the inset in Fig. 5b that, for C1, there is often a disagreement between calculation and experiment on the sign of the hyperfine coupling constant when the latter becomes small. Fig. 5c and d show similar plots for the ^{1}H resonances, with excellent agreement between experiment and calculation for most resonances. The sign of $d\delta_{iso}/d(1/T)$ for H5 is consistently miscalculated, but its magnitude is essentially negligible in both cases. For Hbr, the magnitude of $d\delta_{iso}/d(1/T)$ is calculated to be essentially independent of substituents, but the experimental values show a much wider variation, most likely reflecting that the static picture of the hydrogen-bonded species is incomplete and motion along the O–H$\cdots$O axis may lead to this discrepancy. Initial exploratory calculations confirmed that the chemical shift of this proton may indeed be more sensitive to vibrational averaging than those of most other nuclei (see ESI†), but a full appraisal of the magnitude of this effect would require a proper dynamical treatment (preferably including quantum dynamics), which is beyond the scope of the present paper.

As mentioned above, the gas-phase calculations do not take into account longer-range crystal packing, whereas, in the solid state, a wide range of three-dimensional packing motifs is observed for these compounds.[18] Indeed, two polymorphs are known for **1**[19] (we report data only for the isolated molecular Cu(**L1**)$_2$ complex rather than the polymeric $[Cu(\mathbf{L1})_2]_n$). and we

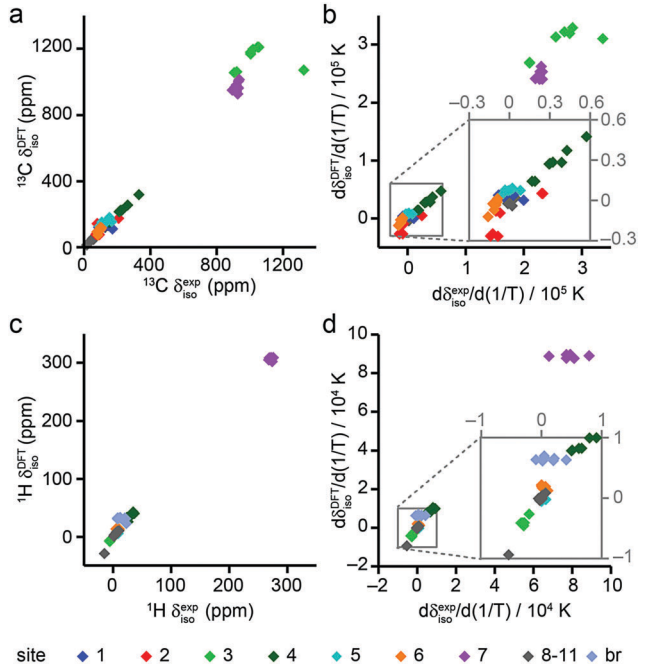

Fig. 5 Plots comparing calculated (DFT) and experimental (exp.) (a) ^{13}C δ_{iso} (at 298 K), (b) ^{13}C $d\delta_{iso}/(1/T)$, (c) ^{1}H δ_{iso} (at 298 K) and (d) ^{1}H $d\delta_{iso}/(1/T)$ for all complexes. *N.B.* as discussed in the text, crystallographic inequivalence was observed for **3**. Average experimental shifts for each C species are reported here – see ESI† for details. Only data for the thermodynamically-stable polymorph of **7** are included.

have also observed polymorphism in **7**, which has a dramatic effect on the observed NMR parameters.[18] The effects of such bulk differences in the crystal structure will be the subject of a subsequent publication and here we report results only for the thermodynamically-stable form of **7**. On a more local level, crystallographic inequivalence of chemically-equivalent species can also lead to small shift differences. Most of the complexes studied here are centrosymmetric, leading to one resonance per chemically-distinct C or H. However, for **3**, multiple resonances are observed for some H species, suggesting either a lowering of the symmetry for the molecule or multiple distinct molecules per unit cell. This is, as might be expected, most apparent for H7, which exhibits two resonances with a shift difference of 9.4 ppm at 298 K (see ESI†). Clearly, such structural effects will, ultimately, need to be considered in order to provide a complete spectral assignment in cases where there are multiple phases or more than one crystallographic ligand species present. We are currently investigating whether these effects can be modelled simply by the interaction within a small (2–3 molecule) cluster, or whether the full periodic crystal structure must be considered.

The combined computational and experimental strategy presented here allows for the assignment of the ^{1}H and ^{13}C NMR spectra of these paramagnetic complexes, with the portion of the molecule closest to the Cu^{2+} centre experiencing large contact shifts and the atoms further away experiencing only much smaller pseudocontact shifts. Given the unexpectedly small paramagnetic shifts for the two C closest (through space and through bond) to the Cu^{2+}, however, DFT calculations are essential for enabling spectral assignment. Our computational method appears generally applicable to these complexes and we are now seeking to extend it to multinuclear complexes more closely resembling the extended structures of MOFs, in order to develop our joint computational/experimental NMR approach into a structural tool for these more demanding materials.

This work was supported by the EPSRC through the Collaborative Computational Project on NMR Crystallography (CCP-NC), *via* EP/M022501/1. SEA would also like to thank the Royal Society and Wolfson Foundation for a merit award. MB would like to thank EaStCHEM and the School of Chemistry for support and access to a computer cluster maintained by Dr H. Früchtl. ZK gratefully acknowledges a scholarship from the China Scholarship Council. For research data supporting this publication see DOI: http://dx.doi.org/10.17630/9061ace0-88fb-4a55-a1eb-05e020f369fd.

Conflicts of interest

There are no conflicts to declare.

References

1 I. Bertini, L. Emsley, M. Lelli, C. Luchinat, J. Mao and G. Pintacuda, *J. Am. Chem. Soc.*, 2010, **132**, 5558.
2 D. M. Dawson, L. E. Jamieson, M. I. H. Mohideen, A. C. McKinlay, I. A. Smellie, R. Cadou, N. S. Keddie, R. E. Morris and S. E. Ashbrook, *Phys. Chem. Chem. Phys.*, 2013, **15**, 919.
3 F. Gul-E-Noor, B. Jee, A. Pöppl, M. Hartmann, D. Himsl and M. Bertmer, *Phys. Chem. Chem. Phys.*, 2011, **13**, 7783.
4 G. de Combarieu, M. Morcrette, F. Millange, N. Guillou, J. Cabana, C. P. Grey, I. Margiolaki, G. Férey and J.-M. Tarascon, *Chem. Mater.*, 2009, **21**, 1602.
5 D. S. Middlemiss, A. J. Ilott, R. J. Clément, F. C. Strobridge and C. P. Grey, *Chem. Mater.*, 2013, **25**, 1723.
6 M. Bühl, S. E. Ashbrook, D. M. Dawson, R. A. Doyle, P. Hrobárik, M. Kaupp and I. A. Smellie, *Chem. – Eur. J.*, 2016, **22**, 15328.
7 N. P. Wickramasinghe, M. A. Shaibat, C. R. Jones, L. B. Casabianca, A. C. de Dios, J. S. Harwood and Y. Ishii, *J. Chem. Phys.*, 2008, **128**, 052210.
8 I. Bertini, *Coord. Chem. Rev.*, 1996, **150**, 1.
9 M. Bertmer, *Solid State Nucl. Magn. Reson.*, 2017, **81**, 1.
10 S. S.-Y. Chui, S. M.-F. Lo, J. P. H. Charmant, A. G. Orpen and I. D. Williams, *Science*, 1999, **283**, 1148.
11 C. Bonhomme, C. Gervais, F. Babonneau, C. Coelho, F. Pourpoint, T. Azaïs, S. E. Ashbrook, J. M. Griffin, J. R. Yates, F. Mauri and C. J. Pickard, *Chem. Rev.*, 2012, **112**, 5733.
12 T. Charpentier, *Solid State Nucl. Magn. Reson.*, 2011, **40**, 1.
13 S. E. Ashbrook and D. McKay, *Chem. Commun.*, 2016, **52**, 7186.
14 S. Moon and S. Patchkovskii, in *Calculation of NMR and EPR Parameters. Theory and Applications*, ed. M. Kaupp, M. Bühl and V. G. Malkin, Wiley-VCH, Weinheim, 2004, pp. 325–340.
15 P. Hrobarik, R. Reviakine, A. V. Arbuznikov, O. L. Malkina, V. G. Malkin, F. Koehler and M. Kaupp, *J. Chem. Phys.*, 2007, **126**, 024107.
16 G. Kervern, G. Pintacuda, Y. Zhang, E. Oldfield, C. Roukoss, E. Kuntz, E. Herdtweck, J.-M. Basset, S. Cadars, A. Lesage, C. Copéret and L. Emsley, *J. Am. Chem. Soc.*, 2006, **128**, 13545.
17 Y. Zhang, H. Sun and E. Oldfield, *J. Am. Chem. Soc.*, 2005, **127**, 3652.
18 F. M. Mack, MChem thesis, University of St Andrews, 2017.
19 K. N. Lazarou, A. K. Boudalis, V. Psycharis and C. P. Raptopoulou, *Inorg. Chim. Acta*, 2011, **370**, 50.